Activated Dissociation of CO$_2$ on Rh(111) and CO Oxidation Dynamics

Heather L. Abbott and Ian Harrison*

Department of Chemistry, University of Virginia, Charlottesville, Virginia 22904-4319

*Received: May 14, 2007; In Final Form: June 27, 2007*

The activated dissociative chemisorption of CO$_2$ on Rh(111) is characterized theoretically with the aid of detailed balance simulations of the CO$_2$ product state distributions measured in thermally driven CO oxidation experiments. A two-parameter formulation of the physisorbed complex−microcanonical unimolecular rate theory (PC−MURT), a local hot spot model for the CO$_2$ gas-surface reactivity, is used to calculate CO$_2$ dissociative sticking coefficients, as well as the angular yields, mean translational energies, and rovibrational energy distributions of desorbing CO$_2$ product from CO oxidation. Measured CO$_2$ product angular yields and infrared chemiluminescence from CO oxidation are consistent with two parallel mechanisms for activated CO$_2$ dissociative chemisorption on Rh(111): a direct mechanism and an indirect mechanism involving a thermalized intermediate. The PC−MURT describes the direct mechanism that is favored at low coverage and helps to reveal the indirect mechanism that can be a substantial reaction pathway (e.g., 65%) under other conditions. For the direct mechanism, simulations of diverse experimental data indicate that the reaction threshold energy for CO$_2$ dissociative chemisorption is $E_0 = 73$ kJ/mol, two surface oscillators participate in the dissociative transition state, and molecular rotation is approximately a spectator to the dissociation dynamics. Accordingly, an experimentally consistent activation energy for CO oxidation via Langmuir−Hinshelwood reaction kinetics is $E_a' \sim 99$ kJ/mol.

1. Introduction

Societal concerns about global warming have heightened scientific interest in achieving a molecular level understanding of CO$_2$ activation on catalytic metal surfaces. Increased use of CO$_2$ as a chemical feedstock for the production of methanol, urea, and other organic molecules could reduce net CO$_2$ emissions and provide a favorable alternative to sequestration of this greenhouse gas, which is an end product of hydrocarbon combustion.[1−3] The dissociation of CO$_2$ is a highly endothermic process in the gas phase ($\Delta H_f°(298$ K$) = 393.5$ kJ/mol)[4] and a substantial activation energy is still required to dissociatively chemisorb this molecule (i.e., CO$_{2(g)} \rightarrow$ CO$_{(c)}$ + O$_{(c)}$) on transition metal catalysts. Only a few experiments have been performed which directly measure dissociative sticking coefficients for CO$_2$ on single-crystal metal surfaces.[5−8] Madix and co-workers measured the dissociative sticking coefficient for CO$_2$ on Ni(100) as a function of translational energy $S(E_t)$ using a nonequilibrium supersonic molecular beam.[5] Averaging their molecular beam derived $S(E_t)$ over a thermal Maxwell−Boltzmann distribution, they calculated a thermal activation energy of only 12 kJ/mol, a value substantially lower than the 89 kJ/mol directly measured by Peebles et al.[7] under high-pressure thermal equilibrium conditions (i.e., 96 Torr H$_2$ and 1 Torr CO$_2$). Similar high pressure measurements[8] of thermal dissociative sticking coefficients for CO$_2$ on Rh(111) yielded an activation energy of 71 kJ/mol. Because CO$_2$'s thermodynamic stability makes it difficult to activate, its dissociation is likely to be rate limiting for catalytic processes that use CO$_2$ as a reagent. A quantitative model of CO$_2$ activation at metal surfaces is desired because of its potential utility in engineering catalytic schemes that use CO$_2$ as a chemical feedstock, particularly in industrial applications that might help reduce atmospheric levels of CO$_2$.

Despite the paucity of experiments investigating CO$_2$ dissociative sticking, the reverse process, CO oxidation, has been extensively studied.[9] CO oxidation is a model reaction for Langmuir−Hinshelwood (L-H) kinetics in which gas-phase reactants are chemisorbed and thermalized prior to products being collisionally formed on the surface. The L-H kinetics may be written as

$$\text{CO}_{(c)} + \text{O}_{(c)} \rightleftarrows \text{CO}_{2(g)} \qquad (1)$$
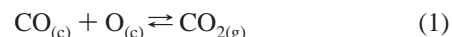
where the reverse process is the dissociative chemisorption of CO$_2$. The eq 1 reactions share a common transition state and face substantial activation barriers. CO oxidation is industrially important as an intermediate step in the steam reforming of methane (i.e., in the water−gas shift reaction) as well as in Fischer−Tropsch synthesis. In automobile exhaust systems, CO oxidation is carried out in catalytic converters composed of supported Pt, Pd, and Rh nanoparticles.[9] Considerable experimental work[10−18] and electronic structure calculations[19] have been performed to characterize CO oxidation on Rh(111), but a consistent theoretical model that explains all the dynamical observations for the CO$_{(c)}$ + O$_{(c)} \rightleftarrows$ O$_{2(g)}$ reactive system has not yet emerged. In this paper, we work toward achieving a more unified understanding of these reactions on Rh(111) using detailed balance and a simple, two-parameter, microcanonical transition state theory model for the activated dissociative chemisorption of CO$_2$.

The dynamics of CO oxidation on Rh(111) have been examined by many groups using a wide range of experimental techniques, including molecular beam methods and infrared chemiluminescence. CO$_2$ product angular yield distributions and mean translational energies were measured by Sibener and co-

* To whom correspondence should be addressed. Phone: (434) 924-3639. Fax: (434) 924-3710. E-mail: harrison@virginia.edu.

workers[10-12] at several surface temperatures for which the CO coverage was minimal (i.e., $\theta_{CO} < 0.01$ monolayer (ML) where 1 ML = 1.38×10^{15} cm^{-2} is the Rh(111) surface atom density), but the oxygen coverage varied ($\theta_O \leq 0.1$ ML). The observed angular yield distributions as a function of polar angle ϑ could be decomposed into two components: a $\cos^n \vartheta$ component, sharply peaked around the surface normal with $n \sim 8$ over a temperature range of 500–800 K, associated with CO$_2$ "directly" desorbing with hyperthermal translational energies, and a $\cos \vartheta$ component, associated with CO$_2$ product with translational energies thermalized to the surface temperature T_s. These polar angular yields of CO$_2$ were well described as $P(\vartheta) = a \cos^n \vartheta + (1 - a) \cos \vartheta$ where both a and n may depend on the surface temperature and the coverages of O and CO. Additional angular distributions for desorbing CO$_2$ have been measured using angle-resolved temperature-programmed reaction (TPR) by Matsushima et al.[18] However, these TPR angular distributions were obtained beginning with high initial coverages of CO and O on the Rh(111) surface that may have evolved into island systems under kinetic control. Molecular beam experiments found that the mean translational energies of desorbing CO$_2$ increase as the surface temperature T_s increases and decrease as the polar angle ϑ increases.[11,12] Coulston and Haller[17] employed high-resolution infrared (IR) chemiluminescence emission spectroscopy to determine apparent vibrational and rotational temperatures (T_v^* and T_r^*, respectively) of vibrationally excited CO$_2$ associatively desorbing from a rhodium foil under high O coverage conditions (i.e., $\theta_O = 0.33$ ML) that were higher than T_s. Via detailed balance, the relatively high apparent vibrational temperatures and moderate apparent rotational temperature were interpreted to indicate that both vibrational and rotational energy help to overcome the barrier for CO$_2$ dissociative sticking. The energy collectively partitioned into CO$_2$ rotational and vibrational modes,[17] $\langle E_{vr} \rangle \sim 24.7$ kJ/mol, was found to be approximately equal to the CO$_2$ mean translational energy directed along the surface normal, $\langle E_t(\vartheta = 0°) \rangle = 29.7$ kJ/mol, that was measured independently by Brown and Sibener.[11]

Electronic structure calculations concerning CO oxidation on Rh(111) have primarily investigated the adsorption and surface structures of CO and O. Recent density functional theory (DFT) computations in combination with experimental methods (i.e., photoemission spectroscopy and scanning tunneling microscopy (STM)), indicate that chemisorbed oxygen atoms on Rh(111) are more active than a complete surface oxide layer for the oxidation of CO, though a partial surface oxide layer is an efficient source of atomic oxygen for the rest of the surface.[20] Reflection absorption infrared spectroscopy and temperature programmed desorption (TPD) have been used in combination with DFT to determine that CO is most stable at atop sites, and either hollow sites (low θ_O) or bridge sites (high θ_O) are additionally occupied as the coverage of O is increased on Rh-(111).[21] Other DFT calculations for CO oxidation on Rh(111) also yield atop site chemisorption for CO and a L-H oxidation mechanism.[22] One DFT study of the transition state for CO oxidation on Rh(111) calculates an early barrier (i.e., the barrier to CO$_2$ dissociation is late with a large r$_{CO-O}$ separation = 1.89 Å) and a reaction threshold energy of 99 kJ/mol.[19] Earlier DFT calculations predicted slightly lower threshold energies of 91 kJ/mol[23] and 96 kJ/mol.[24]

Many questions remain concerning the oxidation of CO on transition metals: estimates of the activation energy on Rh-(111) have varied widely depending on the experimental conditions, ranging from 65 kJ/mol[16] to 188 kJ/mol;[18] there is

still debate about whether CO oxidation is a structure sensitive reaction;[16] and while many experimentalists have noted a bimodal angular distribution for CO$_2$ desorption,[11,12,25-29] there has been little discussion or elucidation of the exact reaction mechanism(s) involved and how the observed dynamics are generated. Part of the difficulty in pinning down the details of the CO oxidation dynamics stems from the reaction's sensitivity to adsorbate surface coverage. Under high coverage (e.g., θ_O = 0.25 ML, θ_{CO} = 0.50 ML) and low surface temperature (T_s < 275 K) conditions, STM experiments and Monte Carlo simulations by Volkening and Wintterlin[30] have shown that CO oxidation occurs at the domain boundaries between (2 × 2)O and c(4 × 2)CO islands on Pt(111). Similarly for Rh(111), low-energy electron diffraction has revealed that coadsorbed CO and O segregate into islands.[18] Using angle-resolved TPR, Matsushima et al.[18] concluded that CO$_2$ desorbs from CO oxidized within the interior of O islands around 400 K, whereas CO$_2$ desorbs from either the perimeter or outside of O islands at slightly higher surface temperatures of 400–500 K. The effect of surface coverage on CO oxidation kinetics on Rh(111) has been investigated by TPR measurements where an inhomogeneous distribution of CO and O on the surface alters the TPR desorption kinetics of CO$_2$.[16] These results illustrate the importance of surface coverage on reactivity, especially under low surface temperature conditions, and they may help to explain the bimodal behavior observed for CO oxidation on Rh(111).

To model the CO$_2$ dissociative chemisorption/CO oxidation dynamics on Rh(111), we employ a two-parameter formulation of the microcanonical unimolecular rate theory (MURT) local hot spot model designed to treat activated gas-surface reactivity. The MURT provides quantum state resolved or averaged dissociative sticking coefficients for CO$_2$ on Rh(111). CO$_2$ product state distributions from thermally driven CO oxidation are readily calculated using the principle of detailed balance.[31-33] A goal of this paper is to extract transition state parameters by simulating as diverse a range of experiments as possible to optimally harvest the available experimental information and enhance confidence in the transition state characterization. The MURT is found capable of reproducing the sharply peaked CO$_2$ product angular yield distributions and CO$_2$ translational and internal energy distributions for the direct component of CO oxidation on Rh(111), as well as the thermal CO$_2$ dissociative sticking coefficients[8] measured at 100 Torr pressure. Previously, the MURT has been successfully applied to characterize the activated dissociative sticking dynamics of hydrogen and alkanes on transition metal surfaces [i.e., H$_2$ on Cu(111);[33,34] CH$_4$ on Pt(111),[35-37] Ni(100),[38-40] and Ir(111);[41] and C$_2$H$_6$ on Pt-(111)[42]], and the chemical vapor deposition of semiconductor thin films [i.e., SiH$_4$ on Si(100)[43]]. The MURT model provides statistical baseline predictions for the gas-surface reactivity against which dynamical behavior,[34] including mode specificity,[40] can be clearly identified when it occurs. In the case of CO$_2$ dissociative chemisorption on Rh(111), MURT analysis of diverse experiments indicates that the threshold energy for the direct reaction is E_0 = 73 kJ/mol, two surface oscillators participate in the reactive transition state, and molecular rotation is approximately a spectator to the dissociation dynamics.

2. Physisorbed Complex−Microcanonical Unimolecular Rate Theory (PC−MURT)

The MURT local hot spot model, pictorially represented in Figure 1 and described in detail elsewhere,[35,36,40] assumes that
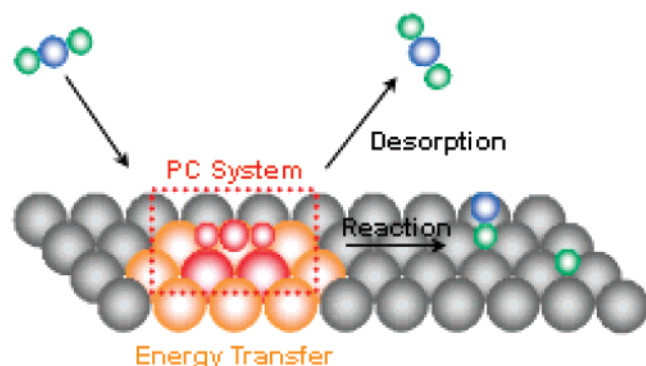
Figure 1. This schematic diagram illustrates the basic premise of the microcanonical unimolecular rate theory (MURT) model: an incident molecule combines with a few surface oscillators to form a transient collision complex or PC system and either reacts or desorbs with energy-dependent RRKM rate constants. Energy exchange with the surrounding bulk metal atoms is neglected in the most basic application of the model, the PC−MURT.

the activated dissociative chemisorption of CO$_2$ can be described microcanonically as

$$CO_{2(g)} \underset{k_D(E^*)}{\overset{F(E^*)}{\rightleftharpoons}} CO_{2(p)} \xrightarrow{k_R(E^*)} CO_{(c)} + O_{(c)} \quad (2)$$
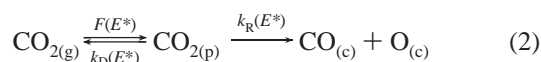
where $k_D(E^*)$ and $k_R(E^*)$ are Rice−Ramsperger−Kassel−Marcus (RRKM) rate constants for desorption and reaction, $F(E^*)$ is the incident flux of collision complexes formed at the surface, surface coordination numbers have been suppressed, and the zero of energy E^* ($= E_t + E_v + E_s$) occurs at 0 K with infinite separation between the surface and CO$_2$. The incident molecule is assumed to interact locally with only a few surface oscillators to form a transient collision complex or physisorbed complex (PC). The PCs do not promptly thermalize to the surface temperature, but rather the energy of the incident molecule and the local surface atoms are presumed to become microcanonically randomized in an ensemble-averaged sense. This energy randomization occurs either by collisional mixing dynamics,[44] rapid intramolecular vibrational energy redistribution, or both.[35] Additional energy transfer between the PCs and the surrounding bulk metal atoms can be modeled using a master equation (i.e., the ME−MURT).[35,36] However, for many small molecule PCs this secondary energy dissipation seems to be relatively slow compared to the ultrafast desorption that competes at the reactive energies of interest. Consequently, the PCs can be approximately treated as being adiabatically isolated using the PC−MURT.[39−41,43]

Applying the steady state approximation to the time dependent coverage of PCs yields an expression for the experimental sticking coefficient

$$S = \int_0^\infty S(E^*)f(E^*) \, dE^* \quad (3)$$

which is an average of the microcanonical sticking coefficient

$$S(E^*) = \frac{W_R^\ddagger(E^* - E_0)}{W_R^\ddagger(E^* - E_0) + W_D^\ddagger(E^*)} \quad (4)$$

where $W_i^\ddagger$ is the sum of states for transition state process i and E_0 is the apparent reaction threshold energy, over the flux distribution of PCs (i.e., the probability that a PC is collisionally formed at energy E^*)

$$f(E^*) =$$
$$\int_0^{E^*} f_t(E_t) \int_0^{E^* - E_t} f_v(E_v) f_s(E^* - E_t - E_v) \, dE_v \, dE_t \quad (5)$$

While the $f(E^*)$ PC flux distribution is straightforwardly fixed by the experimental conditions (i.e., gas and surface temperatures, vibrational frequencies of the incident gas, etc.), the microcanonical sticking coefficient requires additional information about the nature of the reactive transition state that is not as easily gleaned from experimental measurements. Therefore, several transition state parameters must typically be introduced into the PC−MURT model. The principle of detailed balance requires that the incident flux times the dissociative sticking coefficient, which defines the dissociatively chemisorbing flux, must be equal to the associatively desorbing flux under thermal equilibrium conditions (i.e., $FS = D$), even at quantum state-resolved levels of detail. Thus, the principle of detailed balance allows a model of thermal CO$_2$ dissociative chemisorption to predict thermally driven CO oxidation dynamics. In this report, PC−MURT calculations employing detailed balance were used to simulate angular yields, mean translational energies, and rovibrational energy distributions for the CO$_2$ product from CO oxidation.

Two dynamical constraints were applied to the PC−MURT model based on experimental observations. Madix and co-workers found that the dissociative sticking for CO$_2$ on Ni-(100) scales with the normal component of the translational energy based on nonequilibrium supersonic molecular beam measurements.[5,6] The normal translational energy is $E_n = E_t \cos^2 \vartheta$ where ϑ is the angle between the direction of the incident molecules and the surface normal and E_t is the molecular translational energy. In other words, momentum parallel to the surface is apparently conserved until after dissociation. Moreover, CO oxidation experiments monitoring IR chemiluminescence of CO$_2$ product molecules desorbing from a variety of transition metal surfaces measure apparent rotational temperatures that are slightly higher than the surface temperatures [e.g., $T_r^* = 730 \pm 28$ K for $J > 45$ desorbing from a Rh foil at $T_s = 584$ K].[17] The apparent rotational temperatures observed may be somewhat influenced by rotational heating/cooling resulting from collisions with other molecules under the relatively high-pressure conditions above the surface in these supersonic molecular beam experiments in which $\sim 10^{19}$ molecules of CO$_{(g)}$ per cm^2 per second impinge upon the surface. The relatively modest difference between T_r^* and T_s suggests that rotational energy does not greatly assist the process of overcoming the reaction threshold energy E_0 for dissociation. There is some precedent in the literature for rotational energy acting as a spectator degree of freedom in dissociative chemisorption,[45,46,33,34] particularly for H$_2$ on Cu(111).[33,34] In light of the chemiluminescence experiments, we have chosen to treat rotation as a spectator degree of freedom in the PC−MURT calculations presented throughout this paper. Nevertheless, analogous PC−MURT simulations in which rotation was treated as fully participatory in the dissociation dynamics were calculated for comparison and the overall discrepancy with experiments increased only modestly (i.e., by 4%). However, the CO$_2$ product rotational temperature calculated with rotation fully participatory, $T_r^* = 1640$ K, was far too high compared to the $T_r^* = 730 \pm 28$ K value measured at $T_s = 584$ K. The $T_r^* = 584$ K value calculated with rotation as a spectator is much closer to the experimental observations.

Implementation of the PC−MURT requires specification of the desorption and reaction transition states. The desorption transition state is taken to occur when CO$_2$ is freely vibrating

TABLE 1: Transition State Frequencies for CO_2 Dissociation on Pt(111)^a

frequency, ν_i	degeneracy, g_i	approximate assignment
2040 cm^{-1}	1	CO stretch
510 cm^{-1}	1	Pt–CO stretch
420 cm^{-1}	2	CO_2 bend

^{a} Frequencies were obtained from refs 47 and 48. Modes corresponding to parallel translations and frustrated rotations were neglected because parallel translational and rotational motions are assumed to be spectators to the dissociation dynamics.

far from the surface and the surface oscillators are vibrating at the mean phonon frequency of bulk rhodium (i.e., $\nu_s = (3/4) k_B \Theta_{Debye}/h \sim 250$ cm^{-1} where k_B is the Boltzmann constant and $\Theta_{Debye} = 480$ K is the Debye temperature of bulk Rh). The reactive transition state frequencies for CO oxidation on Pt-(111) have been calculated using DFT,[19,47,48] and we presume they are approximately the same for Rh(111). This assumption seems reasonable based on comparison to DFT-calculated adsorption frequencies for CO on Rh(111).[21,49,50] The reactive transition state frequencies for CO oxidation on Pt(111), which are listed in Table 1, have been used for all PC–MURT calculations in this paper. Only the number of surface oscillators s and the apparent reaction threshold energy E_0 remain to be determined, leading to a PC–MURT model with two adjustable parameters. The minimum of the average relative discrepancy (ARD) between the theoretical simulations and experimental observations is used to determine these two parameters by iterative simulation of the available experimental data on Rh-(111) [e.g., CO_2 dissociative sticking coefficients, S]

$$\text{ARD} = \left\langle \frac{|S_{theory} - S_{expt}|}{\min(S_{theory}, S_{expt})} \right\rangle \quad (6)$$

3. Results

The PC–MURT simulations, employing an optimal parameter set of $E_0 = 73$ kJ/mol and $s = 2$, semiquantitatively agree with the experimental data shown in Figures 2–5. This optimal parameter set was determined based on the experimental data depicted in Figures 2, 3a, and 5 (ARD = 20% for these figures) and were used in all the PC–MURT calculations throughout this paper along with the reactive transition state frequencies shown in Table 1. Concurrence between PC–MURT simulations and the CO oxidation experiments shown in Figures 2 and 4 can be obtained by employing a two mechanism model composed of direct (i.e., PC–MURT) and indirect thermal components to describe the associative desorption of CO_2 by detailed balance. The overall ARD for Figures 2, 3a, and 5, which was calculated by weighting each experimental data point equally, strongly depends on the reaction threshold energy E_0 (e.g., when $s = 2$ the overall ARD increases by more than 10% as E_0 varies by ±4 kJ/mol from its minimum value of 73 kJ/mol). Unfortunately, the overall ARD is relatively insensitive to the number of surface oscillators in the physisorbed complex, s (e.g., when $E_0 = 73$ kJ/mol, the overall ARD increases by less than 1% as s goes from 2 to 1 and by less than 3% as s goes from 2 to 3). However, $s = 2$ provides substantially better agreement between the PC–MURT simulated and experimentally observed CO_2 product vibrational energy distribution $P(E_v)$ shown in Figure 4a (e.g., the ARD is ~65% lower for $s = 2$ than $s = 1$).

As illustrated in Figure 2, experimental CO_2 angular yield distributions for CO oxidation on Rh(111) as a function of polar
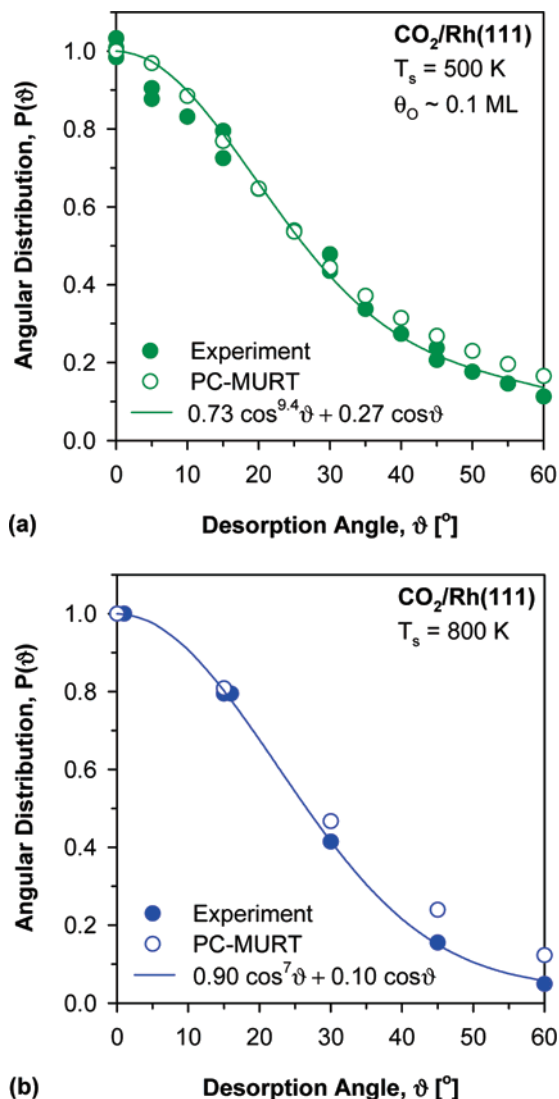

(a)

(b)

Figure 2. Experimental angular distributions (solid points)[11,12] and bimodal fits of the form $P(\vartheta) = a \cos^n \vartheta + (1 - a) \cos \vartheta$ (lines) for desorbing CO_2 product from CO oxidation on Rh(111) are shown for (a) $T_s = 500$ K with $O_{(c)}$ coverage $\theta_O \sim 0.1$ ML and (b) $T_s = 800$ K with unknown θ_O. PC–MURT simulations were substituted into the $P(\vartheta)$ expression above for the direct component (i.e., $\cos^n \vartheta$) to generate values analogous to experiment (open points). The bimodal PC–MURT plus thermal component simulations describe the experimental data with an ARD = 19%.

angle away from the surface normal ϑ have been fit to a bimodal distribution[11,12]

$$P(\vartheta) = a \cos^n \vartheta + (1 - a) \cos \vartheta \quad (7)$$

where a and n are dependent on the surface temperature T_s and oxygen coverage θ_O, and $P(0°) = 1$. The $\cos^n \vartheta$ component has been assigned[12,28] to a direct mechanism yielding hyperthermal CO_2, whereas the $\cos \vartheta$ component has been assigned to an indirect mechanism yielding thermalized CO_2. With the assumption that there is no dependence on azimuthal angle ϕ, the normalized full angular distribution of the desorbing molecular flux $P(\vartheta, \phi)$ when integrated over all out-going solid angles obeys

$$\int \int P(\vartheta, \phi) \cdot d\Omega = \int_0^{2\pi} \int_0^{\pi/2} \left(b \frac{n+1}{2\pi} \cos^n \vartheta + (1 - b) \frac{1}{\pi} \cos \vartheta \right) \cdot \sin \vartheta \, d\vartheta \, d\phi = 1 \quad (8)$$
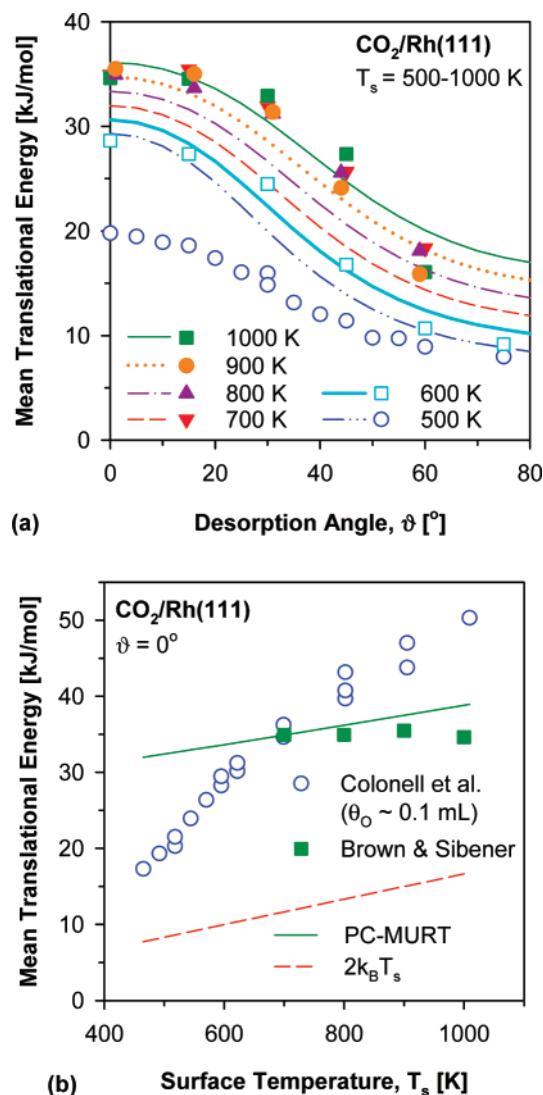
CO$_2$ on Rh(111) and CO Oxidation Dynamics

J. Phys. Chem. C, Vol. 111, No. 35, 2007 **13141**

Figure 3. Mean translational energies for CO$_2$ desorption from Rh-(111) are plotted as a function of (a) desorption angle and (b) surface temperature. (a) PC−MURT simulations (lines) of experimental $\langle E_t(\vartheta) \rangle$ measured by Sibener and co-workers (solid[11,12] and open[11,12] points) have an ARD = 17%. (b) PC−MURT simulations (solid line) of experimental $\langle E_t(T_s) \rangle$ measured by Sibener and co-workers (solid[11,12] and open[11,12] points) have an ARD = 19%. The expectation for a completely thermal mechanism (i.e., $2k_B T_s$) is also shown (dashed line).

where b and $(1 - b)$ are the probabilities for CO oxidation via the direct and indirect mechanisms, respectively. Substituting the PC−MURT simulation for the direct component of the bimodal polar angular distribution of eq 7 allows for direct comparison to experiment as shown in Figure 2 (i.e., the cos^n ϑ term of $P(\vartheta)$ is replaced with the PC−MURT-simulated angular distribution for the direct reaction). The relationship between the a coefficient of the eq 7 polar angular distribution and the b coefficient of the eq 8 full angular distribution is

$$b = \frac{2a}{2a + (1 - a)(n + 1)} \quad (9)$$

Hence, the direct mechanism that figures prominently in the polar angular distributions of Figure 2 accounts for only 34% and 69% (i.e., $b = 0.34$ and 0.69) of the full angular distribution at $T_s = 500$ and 800 K, respectively. The direct mechanism is actually a minority channel until high T_s is reached and the surface coverage of atomic oxygen becomes negligible. The PC−MURT plus cos ϑ bimodal modeling achieves good
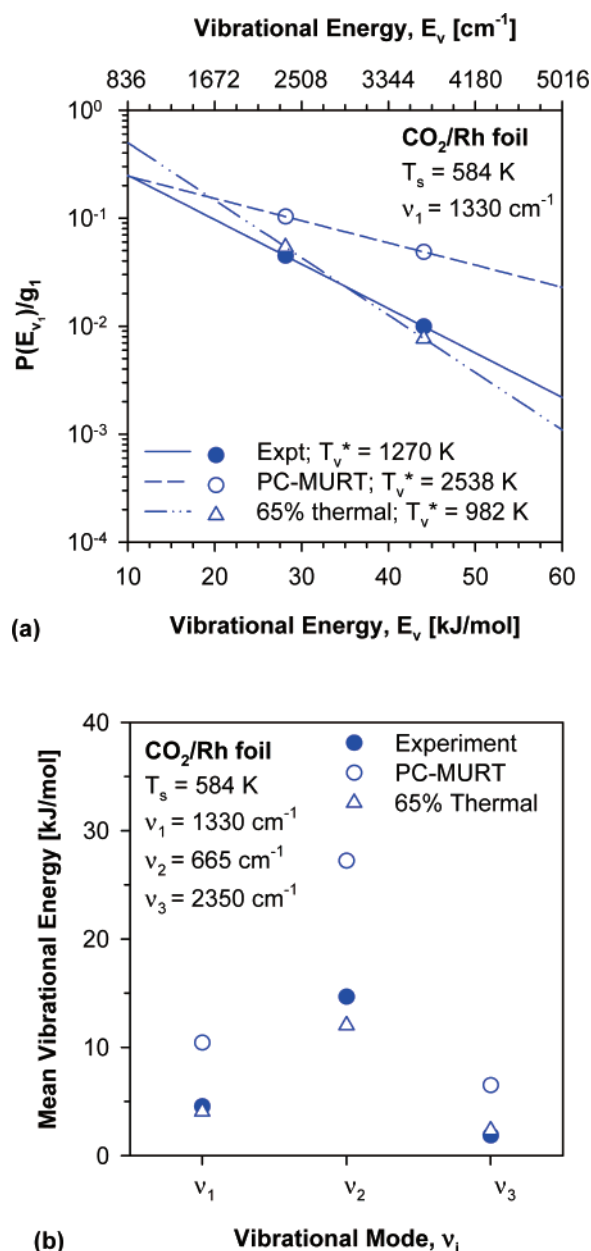

Figure 4. (a) The vibrational energy distribution for CO$_2$ product molecules in the ν_1 mode divided by the vibrational state degeneracy is shown as determined by IR chemiluminescence experiments (solid points)[17] and PC−MURT simulations (open circles). Shown as open triangles, a combination of 65% of the indirect thermal mechanism and 35% of the direct PC−MURT mechanism gave optimal agreement with the experimental distribution for the ν_1 mode. The ARD for the bimodal simulation was 25% whereas for the PC−MURT alone the ARD increased to 261%. The slope of each best fit line defines an apparent vibrational temperature for the ν_1 mode, T_v^*. (b) Experimental mean vibrational energies (solid circles)[17] are plotted as a function of vibrational mode. PC−MURT simulations (open circles) and an optimal combination of 65% indirect and 35% direct mechanism (open triangles) are also shown. The ARD for the bimodal simulation was 20% whereas for the PC−MURT alone the ARD increased to 155%.

agreement with the experimental angular yield distributions to give an ARD of 19%.

Mean translational energies as a function of (a) desorption angle ϑ and (b) surface temperature T_s for CO$_2$ product from CO oxidation on Rh(111) are shown in Figure 3.[11,12] Oxygen coverages were only measured for low surface temperatures, $T_s \leq 600$ K and were found to be $\theta_O \sim 0.1$ ML. The CO$_2$ dynamical measurements at $T_s = 700-1000$ K were likely
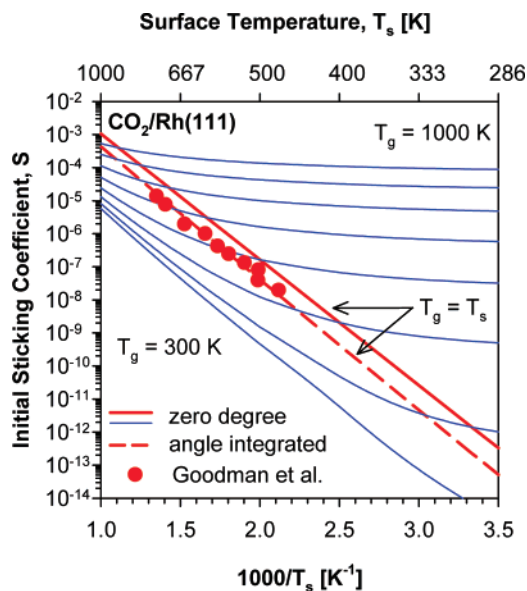
Figure 5. PC−MURT simulations of thermal dissociative sticking coefficients for CO_2 randomly impinging on Rh(111) (dashed bold line) are compared to experimental measurements under relatively high carbon monoxide coverage, θ_{CO}, and low oxygen atom coverage, θ_O, conditions (points).[8] The ARD between the PC−MURT and experimental thermal dissociative sticking coefficients is 30%. The PC−MURT thermal sticking is well fit by an Arrhenius expression, $S(T) = S_0 \exp(-E_a/k_B T)$, where $S_0 = 3.89$ and $E_a = 76$ kJ/mol. Solid lines give PC−MURT predictions for a CO_2 effusive beam incident along the surface normal when $T_g = T_s$ (bold solid line) and $T_g = 300-1000$ K in 100 K increments (thin solid lines).

obtained at lower θ_O. In all cases, we believe that the steady-state CO coverage on the surface was vanishingly small (i.e., $\theta_{CO} < 0.01$ ML). Experimentally derived $\langle E_t(\vartheta)\rangle$ angular distributions at high T_s (i.e., 700−1000 K)[11] shown in Figure 3a depend modestly on the surface temperature and decrease toward $2k_b T_s$ as $\vartheta \rightarrow 90°$ in agreement with PC−MURT simulations. Independent experimental measurements of $\langle E_t(\vartheta,T_s = 500-600K)\rangle$ and $\langle E_t(\vartheta = 0°,T_s)\rangle$ in later experiments[12] from the Sibener laboratory show a more pronounced dependence on the surface temperature that the PC−MURT does not capture as shown in Figure 3b. Although Colonell et al.[12] could fit the broad, single peak time-of-flight (TOF) spectra of the CO_2 product from CO oxidation using a bimodal direct plus thermal components model, sufficient experimental information is not available to simulate these TOF spectra similarly using the PC−MURT for the direct component. Instead, the mean translational energy assuming direct (i.e., PC−MURT) and thermal (i.e., $2k_b T_s$) mechanisms have been shown in Figure 3b. The PC−MURT seems to qualitatively simulate most aspects of the Figure 3 experimental data with improved quantitative success at higher T_s.

IR chemiluminescence experiments[17] measuring the vibrational energy distributions of excited CO_2 product from CO oxidation on a Rh foil, a foil presumably exposing primarily Rh(111) surface facets, find apparent vibrational temperatures T_v^* of the desorbing molecules that are more than twice the surface temperature $T_s = 584$ K (i.e., $T_v^* = 1270 \pm 220$, 1300 ± 60, and 1210 ± 140 K for the ν_1, ν_2, and ν_3 excited states, respectively). However, the PC−MURT model of the direct mechanism alone (i.e., $b = 1$) predicts that desorbing CO_2 molecules should have a T_v^* more than twice the experimentally observed value and four times the surface temperature (cf., T_v^* (PC−MURT) = 2538 K and T_v^* (expt) = 1270 K at $T_s = 584$ K, as shown in Figure 4a for the ν_1 mode of CO_2). The

TABLE 2: Arrhenius Parameters for Thermal Sticking of CO_2 on Rh(111)

	s	S_0	E_a	$S (T = 600$ K$)$
PC−MURT	1	3.78	76 kJ/mol	9.60×10^{-7}
($E_0 = 73$ kJ/mol)	2	3.89	76 kJ/mol	9.70×10^{-7}
	3	3.95	76 kJ/mol	9.75×10^{-7}
experiment[8]		1.28	71 kJ/mol	1.01×10^{-6}

assumption that the vibrational energy distribution of the desorbing molecules derives from the same two mechanisms that give rise to the bimodal angular distribution suggests

$$P(E_v) = bP(E_v,T_v^*) + (1 - b)P(E_v,T_s) \qquad (10)$$

where $P(E_v,T_v^*)$ is the direct PC−MURT component characterized by an elevated vibrational temperature T_v^* and $P(E_v,T_s)$ is the indirect thermal component. Optimizing b for the Figure 4a ν_1 mode experimental $P(E_v)$ observations taken at $T_s = 584$ K results in $b = 0.35$ (i.e., 35% direct) and yields ~235% better agreement with experiment than the PC−MURT predictions alone. An independent value of the b parameter can also be calculated using eq 9 and the experimentally derived values of a and n from the Figure 2a polar angular yield distribution at $T_s = 500$ K (i.e., $a = 0.73$ and $n = 9.4$)[12] to give $b = 0.34$. Agreement between the b coefficients derived from bimodal decomposition of the CO_2 vibrational and angular distributions lends further credence to the idea that the observed CO oxidation proceeds through the two reaction pathways. In Figure 4b, mean vibrational energies determined from the vibrational energy distributions $P(E_v)$ for each vibrational mode of CO_2 illustrate that the PC−MURT alone (i.e., $b = 1$) consistently predicts $\langle E_v\rangle$ values that are higher than experiment (i.e., ARD = 155%). In contrast, $\langle E_v\rangle$ values derived from bimodal distributions with $b = 0.35$ are much more consistent with the experimental observations (i.e., ARD = 20%). The bimodal form for $P(E_v)$ seems reasonable not only because the theoretical simulations are much closer to the observed values using this bimodal distribution but also because earlier experimental analysis[12] has shown that the $P(\vartheta)$ and $P(E_t)$ distributions are similarly bimodal, particularly under these relatively high θ_O conditions.

PC−MURT simulations of thermal dissociative sticking coefficients for randomly impinging CO_2 (bold dashed line) are plotted with high-pressure experimental measurements (points)[8] in Figure 5. Thermal sticking coefficients can be fit well to an Arrhenius expression $S(T) = S_0 \exp(-E_a/k_B T)$ where S_0 is the pre-exponential, and E_a is the activation energy. Table 2 compares the Arrhenius parameters for experiment and the PC−MURT with a variable number of surface oscillators s. As demonstrated in Table 2, the PC−MURT thermal dissociative sticking coefficient is fairly insensitive to the number of surface oscillators under thermal equilibrium conditions. Nonequilibrium effusive molecular beam experiments where surface temperature-dependent dissociative sticking coefficients $S(T_s,T_g)$ are measured at fixed T_g and variable T_s would be more incisive for theoretical determination of s. PC−MURT predictions for such experiments in which T_g varies from 300 to 1000 K in 100 K increments (thin solid lines) are provided in Figure 5. The experimentally derived and PC−MURT simulated thermal dissociative sticking coefficients agree well when the theory is implemented with $E_0 = 73$ kJ/mol and $s = 2$.

Goodman et al.[8] measured turnover frequencies for the dissociation of CO_2 under high-pressure conditions that were designed to minimize θ_O [i.e., 1 Torr of $CO_{2(g)}$ and 99 Torr of $H_{2(g)}$]. Dividing the experimental turnover frequencies by the known impingement rate (i.e., 10^6 CO_2 molecules per Rh atom

CO$_2$ on Rh(111) and CO Oxidation Dynamics

J. Phys. Chem. C, Vol. 111, No. 35, 2007 **13143**

per second at 1 Torr) yielded dissociative sticking probabilities for CO$_2$ on Rh(111). An activation energy of 71 kJ/mol was determined based on an Arrhenius fit to the experimental data. Extrapolating the Arrhenius fit to $T = 300$ K, Goodman and co-workers[8] predicted that the dissociation probability for CO$_2$ on Rh(111) should be less than 10^{-11}. However, these experimental reaction probabilities may represent a lower bound on the dissociative sticking because some of the Rh sites may have been poisoned (i.e., the surface density of available reaction sites might have been smaller than estimated). On the other hand, reasonably, Sibener and co-workers[10,12] were not able to observe dissociative sticking for CO$_2$ molecules in a helium-seeded supersonic molecular beam impinging on Rh(111) with $E_t = 41.5$ kJ/mol at $T_s = 300$ K. The PC−MURT predicts a dissociative sticking coefficient of 5.5×10^{-7} for this experiment assuming a supersonic molecular beam composed of 10% CO$_2$ seeded in He with a nozzle temperature $T_n = 370$ K and a beam translational temperature $T_t = 25$ K. Such a small sticking coefficient (i.e., $<10^{-6}$) is likely below the level of detectability using the helium beam reflectivity method as configured by Sibener and co-workers.[10,12]

4. Discussion

4.A. Reaction Mechanism: Direct versus Bimodal. The PC−MURT simulations of Figures 2 and 4 are consistent with two mechanisms for CO$_2$ dissociative chemisorption on Rh-(111) as evidenced by the presence of direct [i.e., $\cos^n \vartheta$ and $P(E_v,T_v^*)$] and thermal [i.e., $\cos \vartheta$ and $P(E_v,T_s)$] components to the angular yield and vibrational energy distributions of desorbing CO$_2$ product from CO oxidation. Figure 2 plainly shows that the contribution of the direct component of the CO$_2$ product angular yield distribution increases as the surface temperature increases and, perhaps more importantly, as the surface coverage of atomic oxygen decreases. However, the extent to which the thermal mechanism contributes to the experimentally measured mean translational energies shown in Figure 3 is not clear. Nevertheless, improved agreement between the experimental and PC−MURT simulated $\langle E_t(\vartheta,T_s) \rangle$ at $T_s \geq 700$ K suggests that the direct component becomes dominant as T_s increases and θ_O decreases. Because the surface temperature and oxygen coverage are related, it is difficult to ascertain whether the indirect component of the experimental distributions is related to one or both of these parameters. TPD measurements by Root et al.[51] have shown that $2O_{(c)} \rightarrow O_{2(g)}$ desorption begins on Rh-(111) at $T_s \sim 800$ K and continues until $T_s \sim 1325$ K, whereas reaction with CO$_{(c)}$ begins at substantially lower surface temperature (i.e., $T_s < 500$ K) and also increases with temperature. The net implication is that some O is always present on the surface under the experimental conditions of Figures 2−4, but presumably θ_O diminishes monotonically with increasing T_s in these experiments.

Although bimodal CO$_2$ angular yield and translational energy distributions have been observed for CO oxidation on both Rh-(111)[12] and Pt(111),[25] it has been difficult to pin down the molecular-level details responsible for the observed reaction dynamics. Colonell et al.[12] proposed two possible origins for the thermalized CO$_2$ product component observed for CO oxidation on Rh(111). The first scenario posited was that CO$_2$, formed by the reaction of O and CO on the surface, is subsequently trapped by "some geometries", and its molecular energy accommodates before desorption ensues. The transition state for CO oxidation was suggested to be CO$_2^-$-like, an idea to which we will return. Alternatively, Colonell et al.[12] suggested that the presence of an oxide layer could provide a hole through

the reaction barrier, similar to the "barrier with holes" model proposed by Comsa et al.,[52] that might account for the indirect thermal component of the CO$_2$ product observed. If this latter low/no barrier mechanism accounted for the thermal component of the reaction mechanism, then the activation energies for CO oxidation and CO$_2$ dissociative chemisorption measured by experiment would be expected to approach zero, because reactants preferentially follow the lowest-energy pathway on the potential energy surface (PES) unless heavily entropically constrained. Instead, large activation energies have been observed on rhodium surfaces when approaching the reactive transition state from either direction (e.g., $E_a' = 65−188$ kJ/mol for CO oxidation and $E_a = 71$ kJ/mol for CO$_2$ dissociation). In addition, no surface oxide layer on Rh(111) was detected by Colonell et al.,[12] although dissolution of oxygen into the bulk was observed. On the basis of the arguments above, presumably neither a trapping mechanism on a completed surface oxide layer nor a barrier with holes mechanism applies.

The precise role of chemisorbed oxygen atoms in determining the CO oxidation dynamics (i.e., direct versus indirect mechanisms) on Rh(111) at high T_s and moderate θ_O (i.e., $\theta_O \sim 0.1$ ML) has not yet been established.[20] STM images and molecular dynamics simulations have shown that CO oxidation on Pt(111) occurs at the domain boundaries between CO and O islands at high coverage and for surface temperatures less than 275 K.[30] However, such high coverage reaction conditions are likely unusual in high-temperature catalysis involving CO$_2$ dissociation. Kinetic experiments find that a complete (9×9) oxide layer on Rh(111),[20,53] or oxide layers on Pt(111)[54] or Pd nanoparticles,[55] are less effective at oxidizing CO than submonolayer O. The opposite reactivity trend is found for CO oxidation on Pt(110) by STM experiments[56,57] and DFT calculations.[58] Although no surface oxide compound was observed under the conditions of the dynamical CO oxidation experiments on Rh(111), the possibility of small oxygen clusters or a partial oxide monolayer forming on the surface under moderate oxygen coverage conditions is difficult to discount, particularly given the surprising stability of metal oxides at surfaces.[59]

The experimental CO oxidation data on Rh(111) indicate that as T_s increases, the fraction of the CO$_2$ desorbing via the indirect thermal mechanism [i.e., $(1 - b)$] decreases. Colonell et al.[12] note that this is consistent with a trapping mechanism. However, the oxygen atom coverage θ_O also decreases as the surface temperature T_s increases, due to desorption as O$_2$ and reaction with CO, indicating that $(1 - b)$ and θ_O may be directly related. At surface temperatures for which a thermal component is detectable (i.e., $T_s < 800$ K), adjacent atoms or small clusters of oxygen atoms may stabilize a bent CO$_2^-$-like transition state and create a negatively charged intermediate species (e.g., CO$_x^{\delta-}$; $x \geq 3$) that accommodates to the surface temperature and subsequently disproportionates into CO$_{2(g)}$ and a smaller oxygen cluster. Similarly, according to microscopic reversibility, an incident CO$_{2(g)}$ molecule might interact with an oxygen atom or small oxygen cluster to form a carbonate species that then disproportionates into carbon monoxide and a larger oxygen cluster. Noteworthy is that reaction of CO$_2$ with an atomic oxygen-covered Ag(110) surface can produce a stable carbonate species (i.e., CO$_3$)[60−62] with a formal charge of minus one-half according to DFT calculations.[63] Although direct experimental evidence for an ionic intermediate in CO oxidation on Rh(111) is lacking, DFT calculations performed by Ackermann et al.[64] indicate that the catalytically active commensurate oxide structure experimentally observed on Pt(110) is stabilized by the presence of carbonate anions (i.e., CO$_3^{2-}$ or CO$_3^{\delta-}$).

Additional experiments that might identify carbonate intermediates or related species formed during CO_2 dissociative chemisorption on Rh(111) would be desirable to further explore the viability of this mechanism.[65−67]

While bimodal behavior is observed for the CO_2 product angular yield and vibrational energy distributions of Figures 2 and 4, the Figure 3 CO_2 product mean translational energies $\langle E_t(\vartheta, T_s)\rangle$ at high T_s and the Figure 5 thermal dissociative sticking of CO_2 $S(T)$ are well described by a direct mechanism alone (i.e., the PC−MURT simulation; $b = 1$). Agreement between the angle-dependent experimental and PC−MURT mean translational energies is best at the highest surface temperatures ($T_s = 800−1000$ K), conditions for which θ_O is approaching zero and a direct mechanism is expected to dominate the reactivity. Equation 9 applied to the data of Figure 2 shows that the fraction of the CO_2 product attributable to the direct mechanism increases from 34% at $T_s = 500$ K to 69% at $T_s = 800$ K. The thermal dissociative sticking coefficients of Figure 5 were obtained for CO_2 at $T = 450−750$ K under a high background pressure of hydrogen gas (i.e., 99 Torr of H_2) intended to minimize the oxygen atom coverage on the surface by facile reaction to form water. The ability of the PC−MURT alone to reproduce the experimental thermal dissociative sticking data under low θ_O conditions, even at moderate temperatures, supports the postulate that the indirect thermal mechanism depends on the atomic oxygen coverage and not the surface temperature.

4.B. Role of Rotation. The apparent rotational temperature of $T_r^* = 730 \pm 28$ K was measured for the $J > 45$ states of CO_2 product from CO oxidation on a Rh foil at $T_s = 584$ K using IR chemiluminescence[17] and was found to be higher than the surface temperature, but only modestly so. By detailed balance, the higher apparent rotational temperature as compared to the surface temperature for the desorbing CO_2 product indicates that rotation helps to surmount the activation barrier for the reverse process, CO_2 dissociative chemisorption. That is, in thermal equilibrium at an overall temperature $T = T_s = T_g$ the CO_2 molecules that successfully react are a subset characterized by $T_r^* > T_s$. If rotation is a spectator to the direct dissociation, then $T_r^* = T_s$ should apply and, of course, $T_r^* = T_s$ applies for dissociation via the indirect thermal mechanism. PC−MURT calculations for the direct reaction (i.e., with $b = 1$) that assume rotational energy fully participates in overcoming E_0 predict a rotational temperature T_r^* (PC−MURT) = 1640 K, which is more than twice the experimental one, T_r^* (expt) = 730 ± 28 K. Employing a bimodal simulation as done above for the apparent vibrational temperature lowers the apparent rotational temperature to $T_r^* = 1470$ K with rotations fully active whereas $T_r^* = 584$ K with rotations inactive. Thus, the PC−MURT calculations suggest that rotation is more nearly a spectator degree of freedom, rather than being fully participatory, in the dissociation dynamics of CO_2 on Rh(111).

It is plausible that gas-phase translational to rotational or rotational to rotational collisional energy transfer may have influenced the apparent rotational temperature of the desorbing CO_2.[68−71] The chemiluminescence experimentalists[17] conservatively estimate that 65% of the CO_2 molecules detected had at most a single gas-phase collision with the CO supersonic molecular beam flux of 6.7×10^{18} molecules per cm^2 per second impinging on the surface or with the ambient O_2 gas. Although it would be reassuring if lower pressure CO oxidation measurements could be performed to eliminate any ambiguity about possible rotational cooling or heating of the CO_2 product, the finding of a product rotational temperature fairly close to the

surface temperature for an activated surface reaction is not uncommon. Such behavior is consistent with rotation being approximately a spectator to the CO_2 dissociative chemisorption dynamics.

Other activated dissociative chemisorption systems for which rotational energy does not appear to substantially promote reactivity include CH_4 on Ni(100),[45] H_2 on Cu(111),[32−34,72] and N_2 on Cu(111).[46] Experimentally measured dissociative sticking coefficients for CH_4 impinging on Ni(100) from a supersonic molecular beam have shown that rotational excitation by $\Delta J = 2$ enhances reactivity by less than a factor of 2.[45] This experimental finding that increased rotational energy does not lead to a large dynamical enhancement of the sticking contradicts four-dimensional quantum mechanical calculations[73] inclusive of rotations that predict about an order of magnitude enhancement in the dissociative sticking coefficient with modest rotational excitation (i.e., $\Delta J = 2$; $\Delta E_r = 2.3$ kJ/mol). Experiments[32,72] and PC−MURT analysis[33,34] for H_2 on Cu(111) show that rotation is approximately a spectator to the dissociative sticking and recombinative desorption dynamics at thermally accessible energies (i.e., for $E_r \leq 40$ kJ/mol). For the associative recombination of N_2 from Cu(111) at $T_s = 700$ K,[46] apparent rotational temperatures of 910 ± 50 K ($\nu = 0$) and 850 ± 250 K ($\nu = 1$) have been observed suggesting, by detailed balance, that rotational energy may be only weakly involved in the N_2 dissociative chemisorption dynamics. Consequently, the assumption in this paper that rotational energy is approximately a spectator to the dissociative chemisorption dynamics of CO_2 on Rh(111) is not unreasonable.

4.C. Activation Energy for the Dissociative Chemisorption of CO_2. Fairly close agreement between the $E_a = 71$ kJ/mol activation energy measured by Goodman et al.[8] and the $E_a = 76$ kJ/mol value calculated by the PC−MURT supports the optimized reaction threshold energy of $E_0 = 73$ kJ/mol. This E_0 can also be corroborated using knowledge of experimentally measured values for related processes. Figure 6 shows a schematic depiction of the two-dimensional (2D) PES for CO_2 dissociation (as read from left to right) and CO oxidation (as read from right to left) on Rh(111), with the surface degrees of freedom suppressed for clarity. The mean energies of the flux-weighted gas-phase species and the chemisorbed species are also identified on the diagram (dashed lines). CO_2-activated dissociation and CO oxidation share a common reactive transition state with energy $\langle E^*\rangle_R$, the mean energy of the successfully reacting species from either side of the reaction barrier (dotted line). Similarly, the mean energy of the reactant species for desorption and CO oxidation (i.e., $CO_{(c)}$ and $O_{(c)}$) have a common mean energy as depicted by the lowest dashed line in Figure 6.

The activation and desorption energies shown in Figure 6 can be determined by applying an Arrhenius expression to experimentally measured thermal dissociative sticking coefficients [i.e., $S(T) = S_0 \exp(-E_a/RT)$] or desorption rates [i.e., $k(T) = k_0 \exp(-E_d/RT)$], respectively. Within the PC−MURT formulism, these activation and desorption energies can be directly related to the mean energy of the successfully reacting species $\langle E^*\rangle_R$ and the mean energy of all the reactants $\langle E^*\rangle$ by the Tolman expression[74] or $E_a(T) = \langle E^*(T)\rangle_R - \langle E^*(T)\rangle$ as illustrated in ref 35 for activated dissociative sticking. Thus, the activation energy for CO_2 dissociative chemisorption E_a is the energy difference between the mean energy of the successfully reacting PCs and the mean energy of all the PCs formed. Likewise, the activation energy for CO oxidation E_a' is the energy difference between (i) the mean energy of the success-
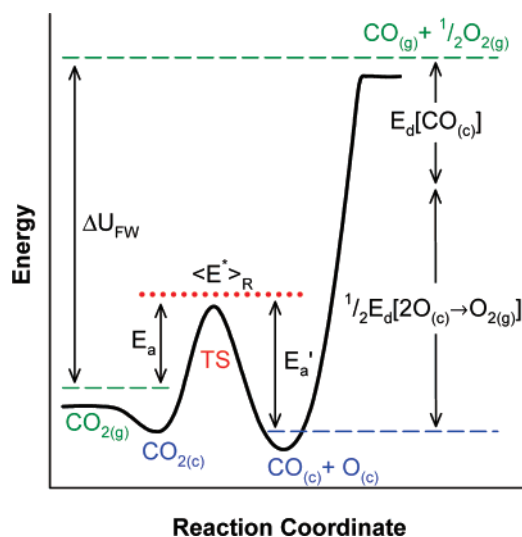
CO2 on Rh(111) and CO Oxidation Dynamics

J. Phys. Chem. C, Vol. 111, No. 35, 2007 **13145**

Figure 6. The 2D potential energy surface for CO_2 dissociation (left to right) and CO oxidation (right to left) via a Langmuir–Hinshelwood reaction mechanism are shown (sold line). Mean energies for the reactant species (dashed lines) and for the common transition state (dotted line) are also identified. Surface coordination numbers have been omitted. Recommended experimental values for use with eq 11 are $\Delta U_{FW} = \Delta H_{600K}^{1bar} + (3/4)RT = 292$ kJ/mol,[4] $E_a' = 102$ kJ/mol,[10] $E_d[CO_{(c)}] = 134$ kJ/mol,[77,78] and $E_d[2O_{(c)} \rightarrow O_{2(g)}] = 356$ kJ/mol[51] that yield $E_a = 82$ kJ/mol for CO_2 dissociative chemisorption on Rh(111). This activation energy compares favorably to Goodman et al.'s experimental value[8] of E_a (600 K) = 71 kJ/mol and the PC–MURT derived value of E_a (600 K) = 76 kJ/mol.

fully reacting $CO_{(c)}$ and $O_{(c)}$ plus some number of adjacent surface atoms s' and (ii) the mean energy of all the $CO_{(c)}$ and $O_{(c)}$ plus s'. Each desorption energy (i.e., $E_d[CO_{(c)}]$ and $E_d[2O_{(c)} \rightarrow O_{2(g)}]$) is equal to the energy difference between the mean energy of the chemisorbed species (i.e., $CO_{(c)}$ and $O_{(c)}$) and the mean energy of the flux-weighted thermal distribution of the successfully desorbing species (i.e., $CO_{(g)}$ and $O_{2(g)}$), assuming constant sticking coefficients for adsorption (i.e., there is no activation barrier to adsorption). The assumption that CO adsorption on Rh(111) is a nonactivated process is confirmed by the experimentally observed cosine angular distribution for thermally desorbing CO.[75] It may be that O_2 dissociative chemisorption on Rh(111) is modestly activated,[76] but below in eq 11 we approximate that the O_2 chemisorption is not activated.

The energy cycle illustrated in Figure 6 can be completed if the total energy difference between the flux-weighted (FW) gas-phase molecules ΔU_{FW} is known. Thus, the activation energy for CO_2 dissociative sticking E_a can be calculated with the equation

$$E_a = \Delta U_{FW} + E_a' - E_d[CO_{(c)}] - (1/2)E_d[2O_{(c)} \rightarrow O_{2(g)}] \quad (11)$$

where ΔU_{FW} is the $CO_{2(g)}$ dissociation energy for flux-weighted reactive and end product distributions, E_a' is the activation energy for CO oxidation, $E_d[CO_{(c)}]$ is the desorption energy for CO, and $E_d[2O_{(c)} \rightarrow O_{2(g)}]$ is the energy for the recombinative desorption of chemisorbed oxygen atoms into gas-phase molecular oxygen. Generally, the energy of reaction for gas-phase dissociation ΔU is equal to the enthalpy change for the gas-phase reaction ΔH plus the work due to the expansion of the gas ΔnRT (i.e., $\Delta U = \Delta H + \Delta nRT$ where $\Delta n = 1/2$ for $CO_{2(g)} \rightarrow CO_{(g)} + (1/2)O_{2(g)}$). The enthalpy of reaction for the dissociation of a three-dimensional (3D) ambient gas ΔH_{3D} can

be obtained from published thermodynamic tables.[4] However, a net correction factor of $(1/4)RT$ for this reaction is necessary to account for the mean translational energy difference between the FW thermal gases and the 3D ambient thermal gases (cf. $\langle E_t \rangle_{FW} = 2RT$ versus $\langle E_t \rangle_{3D} = (3/2)RT$ per mole of gas). Thus, the energy of dissociation for a flux-weighted distribution of gas ΔU_{FW} can be written in terms of the enthalpy of reaction for a 3D ambient gas

$$\Delta U_{FW} = (\Delta H_{3D} + (1/4)RT) + (1/2)RT = \Delta H_{3D} + (3/4)RT \quad (12)$$

Additionally, eq 11 presumes that the number of degrees of freedom is conserved for the reactive transition state from either direction along the Figure 6 PES and that the mean surface energy $\langle E_s(T_s) \rangle$ supplied by the surface oscillators contributes equally to both activation energies, E_a and E_a'.

Reported values of the activation energy for CO oxidation on Rh(111) E_a' have varied considerably from 65 ± 5 kJ/mol[16] to 188 kJ/mol[18] depending on the coverage conditions and the experimental method used. Hopstaken and Niemantsverdriet[16] have compiled a table that summarizes the experimental findings for several rhodium surfaces under a variety of experimental conditions. Goodman and co-workers[13,14] determined the activation energy for CO oxidation using steady-state production of CO_2 under low θ_O and high θ_{CO} conditions and found $E_a = 106$ kJ/mol, a value intermediate among the range in the literature. Brown and Sibener[10] have calculated a similar activation energy of 102 ± 2 kJ/mol based on molecular beam reactive scattering measurements under both high θ_O and low θ_O conditions when $T_s = 500-550$ K. These experimental E_a' values[10,13,14] are also in agreement with Eichler's value[19] of the reaction threshold energy for CO oxidation E_a' (0 K) = 99 kJ/mol calculated using generalized gradient approximation–density functional theory.

While there is general agreement about the desorption energy for CO on Rh(111) (i.e., $E_d[CO_{(c)}] = 134$ kJ/mol at $T_s \sim 500$ K),[77,78] there are conflicting reports about the energy of desorption for $2O_{(c)} \rightarrow O_{2(g)}$ on Rh(111).[51,79,80] Initial measurements[80] of $E_d[2O_{(c)} \rightarrow O_{2(g)}]$ as a function of oxygen coverage were performed using TPD. With the assumption of second order behavior for the oxygen TPD and extrapolating to zero surface coverage, the molecular desorption energy $E_d[2O_{(c)} \rightarrow O_{2(g)}]$ was estimated to be 234 ± 8 kJ/mol. This result seems low based on scatter in the experimental data (refer to Figure 2 of ref 80), including a measurement of $E_d[2O_{(c)} \rightarrow O_{2(g)}] \sim 250$ kJ/mol at $\theta_O < 0.1$ ML. Thiel et al.[80] remarked that dissolution of oxygen into the bulk actually predominated over $O_{2(g)}$ desorption under low-coverage conditions, creating challenges for determining the desorption energy. Later, TPD measurements of the desorption energy on Rh(100) and Rh(111) by Fisher and co-workers[51] found $E_d[2O_{(c)} \rightarrow O_{2(g)}] = 356$ kJ/mol and a desorption temperature of ~ 1300 K. Fisher and co-workers[51] did not observe any dissolution of oxygen into rhodium but noted that carbon was introduced into the crystal by sputtering. Before measuring $E_d[O_{2(c)}]$, they heated the crystal to 1100 K in 3×10^{-8} Torr $O_{2(g)}$ for several hours until the TPD spectra showed no high-temperature CO peak. On the basis of the experimental precautions taken in Fisher's experiments,[51] a treatment that did not oxidize the rhodium surface, the value of $E_d[2O_{(c)} \rightarrow O_{2(g)}] = 356$ kJ/mol seems the most robust and will be used below in our thermodynamic calculation of E_a for CO_2 dissociation.

The activation energy for CO_2 dissociation on Rh(111) can be computed by substituting experimental values from the
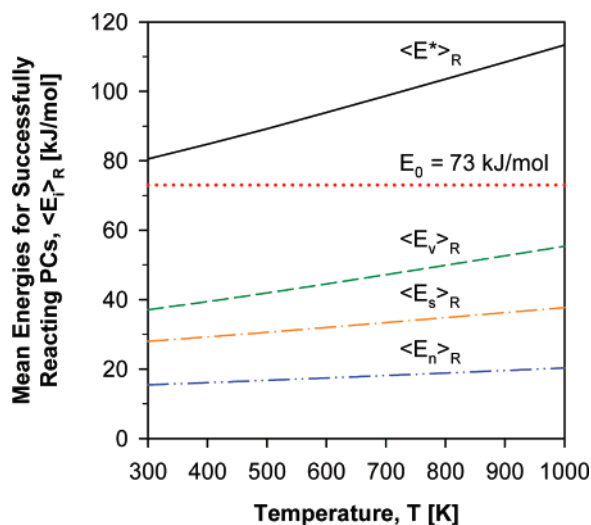
Figure 7. Mean energies derived from different degrees of freedom for the successfully reacting physisorbed complexes $\langle E_i \rangle_R$ are graphed as a function of temperature for CO_2 dissociative chemisorption under thermal equilibrium conditions. The reaction threshold energy E_0 is also indicated.

discussion above into eq 11. Summing the enthalpy of reaction for the dissociation of ambient $CO_{2(g)}$ $\Delta H_{3D} = \Delta H_{600K}^{1bar} \sim 288$ kJ/mol[4] and the total correction term $(3/4)RT \sim 4$ kJ/mol at $T = 600$ K yields the total energy change for the dissociation of flux-weighted $CO_{2(g)}$ $\Delta U_{FW} = 292$ kJ/mol. Through the use of the experimentally measured desorption energies $E_d[CO_{(c)}] = 134$ kJ/mol[77,78] and $E_d[2O_{(c)} \rightarrow O_{2(g)}] = 356$ kJ/mol[51] and the activation energy for CO oxidation $E_a' = 102$ kJ/mol,[10] the activation energy for CO_2 dissociative chemisorption on Rh-(111) is $E_a = 82$ kJ/mol according to eq 11. With the assumption that the calculated activation energy does not vary substantially with temperature, $E_a = 82$ kJ/mol agrees quite well with the activation energies experimentally measured by Goodman et al.[8] [i.e., E_a (600 K) = 71 kJ/mol] and calculated by the PC–MURT [i.e., E_a (600 K) = 76 kJ/mol]. However, alternative literature values for E_a' and $E_d[2O_{(c)} \rightarrow O_{2(g)}]$ result in activation energies E_a that range from 42 to 226 kJ/mol for the dissociation of CO_2. The PC–MURTs ability to reproduce a diverse range of experimental dynamics, including CO_2 product angular yields,[11,12] mean translational energies,[11,12] and internal state distributions,[17] as well as CO_2 dissociative sticking coefficients,[8] provides some confidence, based on experimental consensus, that $E_0 = 73$ kJ/mol appropriately characterizes the dissociative chemisorption of CO_2 on Rh(111). Given $E_0 = 73$ kJ/mol, eq 11 defines the activation energy for CO oxidation on Rh(111) as $E_a' \sim 99$ kJ/mol.

4.D. Fractional Energy Uptakes. Fractional energy uptakes for dissociative chemisorption are defined as the mean energy derived from a particular degree of freedom for those PCs that successfully react divided by the total mean energy for all PCs that successfully react or $f_i = \langle E_i \rangle_R / \langle E^* \rangle_R$. The f_i's identify from which degrees of freedom energy is drawn to overcome the activation barrier for CO_2 dissociative chemisorption. By detailed balance, the f_i's also give the product fractional energy release for CO oxidation, or the fraction of the active exchangeable transition state energy $\langle E^* \rangle_R$ that goes into the surface and CO_2 product energies, $\langle E_i \rangle_R$. Figure 7 shows the mean energies for successfully reacting PCs under thermal equilibrium conditions where CO_2 molecules impinge on the surface randomly from all possible angles. The mean energies, and consequently the fractional energy uptakes, vary little over the temperature range depicted. At 900 K, the molecular vibrational degrees of

freedom $f_v = 49\%$ contribute the preponderance of the energy necessary to surmount E_0 for CO_2 dissociative chemisorption, followed by the two surface oscillators with $f_s = 33\%$, and normal translation with $f_n = 18\%$. Because rotation is treated as a spectator to the reaction dynamics, $f_r = 0\%$. Fractional energy uptakes predicted for CO_2 molecules incident along the surface normal are somewhat different than those predicted for the entire angle-integrated thermal flux distribution (cf., $f_v = 40\%$, $f_s = 29\%$, and $f_n = 31\%$ for $\vartheta = 0°$). For CO oxidation on Pt(111), Allers et al.[29] estimated the product fractional energy release to be $f_{rv} \sim 40\%$, $f_n \sim 40\%$, and $f_s = 20\%$ based on angle-integrated mean rovibrational energies $\langle E_{rv} \rangle$, zero-degree mean translational energies $\langle E_t(\vartheta = 0°) \rangle$, and the assumption of a solely direct reaction mechanism with the CO oxidation exoergicity from the transition state being independent of coverage and surface temperature. The surface energy release of $f_s = 20\%$ was obtained by subtraction. In summary, the PC–MURT thermal equilibrium fractional energy uptakes of $f_v = 49\%$, $f_s = 33\%$, and $f_n = 18\%$ for $CO_2/Rh(111)$ as compared to Allers et al.'s estimates of $f_{rv} \sim 40\%$, $f_s \sim 20\%$, and $f_n \sim 40\%$ for $CO_2/Pt(111)$ indicate heightened importance of molecular vibrations and surface phonons over molecular normal translation in promoting reaction. Within the statistical PC–MURT model, these fractional energy uptakes are reflective of the relative availability of active exchangeable energy from particular degrees of freedom under thermal equilibrium conditions.

The surface contribution toward activating the thermal dissociation of CO_2 on Rh(111) is substantial according to the PC–MURT. Considering the vital role of surface phonons in the dissociative chemisorption of even the lightest molecules, such as H_2,[33,81] it may not be surprising that the surface contributes about a third of the energy necessary for thermal dissociative sticking of the heavier CO_2. From a mechanical viewpoint, the impact of CO_2 on a surface might be expected to excite and couple to phonons more readily than the impact of much lighter H_2. Interestingly, PC–MURT calculations indicate that the fractional energy uptake from the surface is larger for H_2 dissociative chemisorption on Cu(111) [$E_0 = 62$ kJ/mol, $s = 1$][34] than for CO_2 dissociative chemisorption on Rh(111) [$E_0 = 73$ kJ/mol, $s = 2$] under thermal equilibrium conditions (cf., $f_s \sim 40\%$ versus $f_s \sim 30\%$, respectively). This somewhat counterintuitive result arises because reactivity within the framework of the PC–MURT is based on the availability of energy to surmount the reaction threshold energy E_0. Thus, successfully reacting PCs formed for $H_2/Cu(111)$ withdraw relatively more energy from the surface degrees of freedom than those for $CO_2/Rh(111)$ because H_2 has fewer molecular vibrational degrees of freedom that can contribute energy toward surmounting E_0. Relative dissociative sticking coefficients experimentally determined by Murphy and Hodgson[81] via recombinatively desorbing H_2 from Cu(111) in the ($\nu = 0$, $J = 1$) eigenstate have an Arrhenius dependence on the surface temperature with an effective activation energy that can be roughly parametrized as "$E_a(T_s)$" $= 56$ kJ/mol $- 0.92E_n$. Consequently, there is clear-cut experimental evidence for the importance of surface phonons in the activated dissociative chemisorption of even the lightest molecule, particularly at low E_n. In other work, classical trajectory calculations with energy partitioning[82] suggest that 15% of the product energy from CH_4 associative desorption on Ni(111) is channeled into the surface (i.e., $f_s = 15\%$) whereas PC–MURT calculations for CH_4 on Ni(100) at $T = 500$ K yield $f_s = 25\%$. Unfortunately, there have been no nonequilibrium experimental measurements to directly probe the surface temperature dependence of CO_2

CO₂ on Rh(111) and CO Oxidation Dynamics

J. Phys. Chem. C, Vol. 111, No. 35, 2007 **13147**

dissociative chemisorption on Rh(111). Surface phonons are apparently important for CO_2 activated dissociative chemisorption on Rh(111), but the precise extent of their involvement remains somewhat unconstrained by experiments (e.g., $f_s = 20-43\%$ for the $s = 1-3$ values considered in Table 2). Nonequilibrium dissociative sticking measurements $S(T_s, T_g)$, such as those recently measured for CH_4[37] and C_2H_6[42] on Pt(111) and predicted for CO_2 dissociative sticking on Rh(111) in Figure 5, might more definitively restrict the range of viable s values and thereby further clarify the role of the surface.

5. Conclusions

With no more parameters than an Arrhenius rate constant, the PC−MURT is able to semiquantitatively reproduce a wide variety of CO oxidation dynamics (e.g., CO_2 $P(\vartheta)$, $P(E_v)$, and $\langle E_t(\vartheta, T_s) \rangle$) and thermal dissociative sticking measurements for CO_2 on Rh(111). Angular yields and mean translational energies for desorbing CO_2 reaction product as well as CO_2 thermal dissociative sticking coefficients were simulated to characterize the transition state for the direct dissociative chemisorption of CO_2 ($E_0 = 73$, $s = 2$). Molecular rotation was found to be approximately a spectator degree of freedom. The PC−MURT recovers an Arrhenius form for the CO_2 thermal dissociative sticking coefficient, $S(T) = S_0 \exp(-E_a/k_B T)$, where $S_0 = 3.89$ and $E_a = 76$ kJ/mol. The PC−MURT's ability to accurately simulate (i) $\langle E_t(\vartheta, T_s) \rangle$ at high T_s and (ii) $S(T)$ at modest T and high pressures of $H_{2(g)}$, under conditions that prevent O accumulation on the surface, indicates the direct mechanism dominates on the clean surface over a variety of T_s. Hence, the indirect mechanism for CO oxidation and activated CO_2 dissociation on Rh(111) is believed to depend primarily on θ_O rather than T_s and may be facilitated by formation of a thermalized intermediate involving chemisorbed O (e.g., a carbonate species). Fractional energy uptakes calculated by the PC−MURT indicate that molecular vibrations supply the preponderance of energy necessary to surmount E_0 in the thermal dissociative chemisorption of CO_2, followed by energy from surface phonons, and, last, molecular translational energy directed along the surface normal. The activation energy for CO_2 thermal dissociative sticking E_a (600 K) = 76 kJ/mol calculated by the PC−MURT agrees quite well with the E_a (600 K) = 71 kJ/mol value measured by Goodman et al.[8] and the E_a = 82 kJ/mol value calculated via eq 11 using an energetic cycle based on experimental kinetics. Employing the PC−MURT value of $E_a = 76$ kJ/mol in eq 11 yields an activation energy for CO oxidation on Rh(111) of $E_a' \sim 99$ kJ/mol that is in good agreement with some experiments[10,13,14] and electronic structure calculations.[19] As a unified framework for describing the direct CO_2 dissociative chemisorption and CO oxidation on Rh(111), the PC−MURT has provided several insights (e.g., E_0, s, f_i's, and b) into the experimentally observed reaction dynamics. Nevertheless, additional nonequilibrium experiments that directly investigate the roles of surface temperature, rotation, and the formation of a thermalized intermediate species in the dissociative chemisorption of CO_2 and CO oxidation on Rh-(111) as a function of O coverage would be helpful to further clarify the reaction dynamics that can seemingly arise from both direct and indirect reaction mechanisms.

for providing reactive transition state frequencies based on DFT calculations of CO oxidation on Pt(111).

References and Notes

(1) Aresta, M.; Tommasi, I. *Energy Convers. Manage.* **1997**, *38*, S373.
(2) Arakawa, H.; Aresta, M.; Armor, J. N.; Barteau, M. A.; Beckman, E. J.; Bell, A. T.; Bercaw, J. E.; Creutz, C.; Dinjus, E.; Dixon, D. A.; Domen, K.; DuBois, D. L.; Eckert, J.; Fujita, E.; Gibson, D. H.; Goddard, W. A.; Goodman, D. W.; Keller, J.; Kubas, G. J.; Kung, H. H.; Lyons, J. E.; Manzer, L. E.; Marks, T. J.; Morokuma, K.; Nicholas, K. M.; Periana, R.; Que, L.; Rostrup-Nielson, J.; Sachtler, W. M. H.; Schmidt, L. D.; Sen, A.; Somorjai, G. A.; Stair, P. C.; Stults, B. R.; Tumas, W. *Chem. Rev.* **2001**, *101*, 953.
(3) Song, C. S. *Catal. Today* **2006**, *115*, 2.
(4) Chase, M. *J. Phys. Chem. Ref. Data* **1998**, *9*, 1.
(5) D'Evelyn, M. P.; Hamza, A. V.; Gdowski, G. E.; Madix, R. J. *Surf. Sci.* **1986**, *167*, 451.
(6) Gdowski, G. E.; Hamza, A. V.; D'Evelyn, M. P.; Madix, R. J. *J. Vac. Sci. Technol., A* **1985**, *3*, 1561.
(7) Peebles, D. E.; Goodman, D. W.; White, J. M. *J. Phys. Chem.* **1983**, *87*, 4378.
(8) Goodman, D. W.; Peebles, D. E.; White, J. M. *Surf. Sci.* **1984**, *140*, L239.
(9) Chorkendorff, I.; Niemantsverdriet, J. W. *Concepts of Modern Catalysis and Kinetics*; Wiley-VCH Verlag GmbH & Co.: Weinheim, Germany, 2003.
(10) Brown, L. S.; Sibener, S. J. *J. Chem. Phys.* **1988**, *89*, 1163.
(11) Brown, L. S.; Sibener, S. J. *J. Chem. Phys.* **1989**, *90*, 2807.
(12) Colonell, J. I.; Gibson, K. D.; Sibener, S. J. *J. Chem. Phys.* **1995**, *103*, 6677.
(13) Goodman, D. W.; Peden, C. H. F. *J. Phys. Chem.* **1986**, *90*, 4839.
(14) Peden, C. H. F.; Goodman, D. W.; Blair, D. S.; Berlowitz, P. J.; Fisher, G. B.; Oh, S. H. *J. Phys. Chem.* **1988**, *92*, 1563.
(15) Hopstaken, M. J. P.; van Gennip, W. J. H.; Niemantsverdriet, J. W. *Surf. Sci.* **1999**, *435*, 69.
(16) Hopstaken, M. J. P.; Niemantsverdriet, J. W. *J. Chem. Phys.* **2000**, *113*, 5457.
(17) Coulston, G. W.; Haller, G. L. *J. Chem. Phys.* **1991**, *95*, 6932.
(18) Matsushima, T.; Matsui, T.; Hashimoto, M. *J. Chem. Phys.* **1984**, *81*, 5151.
(19) Eichler, A. *Surf. Sci.* **2002**, *498*, 314.
(20) Lundgren, E.; Gustafson, J.; Resta, A.; Weissenrieder, J.; Mikkelsen, A.; Andersen, J. N.; Kohler, L.; Kresse, G.; Klikovits, J.; Biederman, A.; Schmid, M.; Varga, P. *J. Electron. Spectrosc. Relat. Phenom.* **2005**, *144*, 367.
(21) Krenn, G.; Bako, I.; Schennach, R. *J. Chem. Phys.* **2006**, *124*, 144703.
(22) Zhang, A. H.; Zhu, J.; Duan, W. H. *J. Chem. Phys.* **2006**, *124*.
(23) Liu, Z. P.; Hu, P. *J. Chem. Phys.* **2001**, *115*, 4977.
(24) Zhang, C. J.; Hu, P. *J. Am. Chem. Soc.* **2000**, *122*, 2134.
(25) Campbell, C. T.; Ertl, G.; Kuipers, H.; Segner, J. *J. Chem. Phys.* **1980**, *73*, 5862.
(26) Poehlmann, E.; Schmitt, M.; Hoinkes, H.; Wilsch, H. *Surf. Sci.* **1993**, *287*, 269.
(27) Poehlmann, E.; Schmitt, M.; Hoinkes, H.; Wilsch, H. *Surf. Rev. Lett.* **1995**, *2*, 741.
(28) Segner, J.; Campbell, C. T.; Doyen, G.; Ertl, G. *Surf. Sci.* **1984**, *138*, 505.
(29) Allers, K. H.; Pfnur, H.; Feulner, P.; Menzel, D. *J. Chem. Phys.* **1994**, *100*, 3985.
(30) Volkening, S.; Wintterlin, J. *J. Chem. Phys.* **2001**, *114*, 6382.
(31) Cardillo, M. J.; Balooch, M.; Stickney, R. E. *Surf. Sci.* **1975**, *50*, 263.
(32) Rettner, C. T.; Michelsen, H. A.; Auerbach, D. J. *J. Chem. Phys.* **1995**, *102*, 4625.
(33) Abbott, H. L.; Harrison, I. *J. Chem. Phys.* **2006**, *125*, 024704.
(34) Abbott, H. L.; Harrison, I. *J. Phys Chem. A*, in press.
(35) Bukoski, A.; Blumling, D.; Harrison, I. *J. Chem. Phys.* **2003**, *118*, 843.
(36) Bukoski, A.; Abbott, H. L.; Harrison, I. *J. Chem. Phys.* **2005**, *123*, 094707.
(37) DeWitt, K. M.; Valadez, L.; Abbott, H. L.; Kolasinski, K. W.; Harrison, I. *J. Phys. Chem. B* **2006**, *110*, 6705.
(38) Bukoski, A.; Harrison, I. *J. Chem. Phys.* **2003**, *118*, 9762.
(39) Abbott, H. L.; Bukoski, A.; Kavulak, D. F.; Harrison, I. *J. Chem. Phys.* **2003**, *119*, 6407.
(40) Abbott, H. L.; Bukoski, A.; Harrison, I. *J. Chem. Phys.* **2004**, *121*, 3792.
(41) Abbott, H. L.; Harrison, I. *J. Phys. Chem. B* **2005**, *109*, 10371.
(42) DeWitt, K. M.; Valadez, L.; Abbott, H. L.; Kolasinski, K. W.; Harrison, I. *J. Phys. Chem. B* **2006**, *110*, 6714.

(43) Kavulak, D. F.; Abbott, H. L.; Harrison, I. *J. Phys. Chem. B* **2005**, *109*, 685.

(44) Ukraintsev, V. A.; Harrison, I. *J. Chem. Phys.* **1994**, *101*, 1564.

(45) Juurlink, L. B. F.; Smith, R. R.; Utz, A. L. *Faraday Discuss.* **2000**, *117*, 147.

(46) Murphy, M. J.; Skelly, J. F.; Hodgson, A. *J. Chem. Phys.* **1998**, *109*, 3619.

(47) Eichler, A.; Hafner, J. *Phys. Rev. B* **1999**, *59*, 5960.

(48) Eichler, A. Private communication, 2002.

(49) Kohler, L.; Kresse, G. *Phys. Rev. B* **2004**, *70*, 165405.

(50) Curulla, D.; Linke, R.; Clotet, A.; Ricart, J. M.; Niemantsverdriet, J. W. *Phys. Chem. Chem. Phys.* **2002**, *4*, 5372.

(51) Root, T. W.; Schmidt, L. D.; Fisher, G. B. *Surf. Sci.* **1983**, *134*, 30.

(52) Comsa, G.; David, R. *Chem. Phys. Lett.* **1977**, *49*, 512.

(53) Lundgren, E.; Mikkelsen, A.; Andersen, J. N.; Kresse, G.; Schmid, M.; Varga, P. *J. Phys.: Condens. Matter* **2006**, *18*, R481.

(54) Gerrard, A. L.; Weaver, J. F. *J. Chem. Phys.* **2005**, *123*.

(55) Brandt, B.; Schalow, T.; Laurin, M.; Schauermann, S.; Libuda, J.; Freund, H. J. *J. Phys. Chem. C* **2007**, *111*, 938.

(56) Hendriksen, B. L. M.; Frenken, J. W. M. *Phys. Rev. Lett.* **2002**, *89*.

(57) Hendriksen, B. L. M.; Bobaru, S. C.; Frenken, J. W. M. *Top. Catal.* **2005**, *36*, 43.

(58) Pedersen, T. M.; Li, W. X.; Hammer, B. *Phys. Chem. Chem. Phys.* **2006**, *8*, 1566.

(59) Campbell, C. T. *Phys. Rev. Lett.* **2006**, *96*.

(60) Guo, X. C.; Madix, R. J. *Surf. Sci.* **2001**, *489*, 37.

(61) Guo, X. C.; Madix, R. J. *J. Phys. Chem. B* **2001**, *105*, 3878.

(62) Kittel, M.; Sayago, D. I.; Hoeft, J. T.; Polcik, M.; Pascal, M.; Lamont, C. L. A.; Toomes, R. L.; Woodruff, D. P. *Surf. Sci.* **2002**, *516*, 237.

(63) Robinson, J.; Woodruff, D. P. *Surf. Sci.* **2004**, *556*, 193.

(64) Ackermann, M. D.; Pedersen, T. M.; Hendriksen, B. L. M.; Robach, O.; Bobaru, S. C.; Popa, I.; Quiros, C.; Kim, H.; Hammer, B.; Ferrer, S.; Frenken, J. W. M. *Phys. Rev. Lett.* **2005**, *95*, 255505.

(65) Liu, Z. M.; Zhou, Y.; Solymosi, F.; White, J. M. *J. Phys. Chem.* **1989**, *93*, 4383.

(66) Ricart, J. M.; Habas, M. P.; Clotet, A.; Curulla, D.; Illas, F. *Surf. Sci.* **2000**, *460*, 170.

(67) Freund, H. J.; Roberts, M. W. *Surf. Sci. Rep.* **1996**, *25*, 225.

(68) Khan, F. A.; Kreutz, T. G.; Oneill, J. A.; Wang, C. X.; Flynn, G. W.; Weston, R. E. *J. Chem. Phys.* **1990**, *93*, 445.

(69) Roche, C.; Millot, G.; Chaux, R.; Saintloup, R. *J. Chem. Phys.* **1994**, *101*, 2863.

(70) Millot, G.; Roche, C. *J. Raman Spectrosc.* **1998**, *29*, 313.

(71) Deroussiaux, A.; Lavorel, B. *J. Chem. Phys.* **1999**, *111*, 1875.

(72) Michelsen, H. A.; Rettner, C. T.; Auerbach, D. J.; Zare, R. N. *J. Chem. Phys.* **1993**, *98*, 8294.

(73) Carré, M. N.; Jackson, B. *J. Chem. Phys.* **1998**, *108*, 3722.

(74) Tolman, R. C. *J. Am. Chem. Soc.* **1920**, *43*, 2506.

(75) Viste, M. E.; Gibson, K. D.; Sibener, S. J. *J. Catal.* **2000**, *191*, 237.

(76) Artsyukhovich, A. N.; Harrison, I. *Surf. Sci.* **1996**, *350*, L199.

(77) Thiel, P. A.; Williams, E. D.; Yates, J. T.; Weinberg, W. H. *Surf. Sci.* **1979**, *84*, 54.

(78) Peterlinz, K. A.; Curtiss, T. J.; Sibener, S. J. *J. Chem. Phys.* **1991**, *95*, 6972.

(79) Weinberg, W. H. *Surf. Sci.* **1983**, *128*, L224.

(80) Thiel, P. A.; Yates, J. T.; Weinberg, W. H. *Surf. Sci.* **1979**, *82*, 22.

(81) Murphy, M. J.; Hodgson, A. *J. Chem. Phys.* **1998**, *108*, 4199.

(82) Henkelman, G.; Arnaldsson, A.; Jonsson, H. *J. Chem. Phys.* **2006**, *124*, 044706.